JOURNAL OF SPACECRAFT AND ROCKETS
Vol. 34, No. 5, September–October 1997

Plasma and Aerothermal Measurements on a Hypervelocity Re-Entry Vehicle

Kenneth M. Chadwick*
Calspan SRL Corporation, Buffalo, New York 14225

A laboratory measurements program has been performed in the Calspan 96-in. Hypersonic Shock Tunnel, which has provided a database on the effects of an ionized flowfield about a re-entry vehicle on rf propagation. Electron number density measurements were made by using swept-voltage thin-wire electrostatic probes in a rake over the various receiver stations on the bluntnose-cone test vehicle. In addition, aerothermal measurements were made along both leeward and windward sides of the test vehicle at all configurations. Test model orientations included pitch, yaw, and combinations of pitch and yaw, which resulted in test model angles of attack at 0, 2, 6, and 13 deg. The hypersonic test environment corresponded to high-altitude 42.6 km (140,000 ft) re-entry conditions at 4.26 km/s (14,000 ft/s). The simulations produce a laminar flow over the full-scale re-entry vehicle test model.

Nomenclature

I_i = ion current
i_+ = current normalization factor
j = current density
m = mass
n = number density
r = radius
T = temperature
V = voltage potential
ε_0 = vacuum permittivity
λ_D = Debye length
χ_p = nondimensional probe potential

Subscripts

e = electron
F = floating
i = ion
p = probe

Introduction

THE potential for signal quality degradation in electromagnetic propagation through the flowfields surrounding hypervelocity vehicles during re-entry is of specific interest to guidance sensor applications. Aerodynamic phenomena introduce density and temperature gradients into the nonplanar flowfield behind the bow shock, and aerothermal phenomena introduce plasma levels as a result of thermal ionization processes.

Therefore, electromagnetic radiation will experience attenuation, phase shift, and scattering in propagating through such environments. The severity of these effects on guidance performance will depend on the magnitude of the signal frequency relative to the plasma frequency and the collision frequency, as well as their gradients. These plasma–microwave interaction effects will further be rendered more complex by the asymmetry of the flowfield plasma due to vehicle maneuvering. Antenna window heating can also present critical problems in the flight case as high heat transfer rates can initiate softening or melting of the material leading to shape distortion, ablation, and changes in refractive index. Microwave signal processing must account for all of these perturbation effects to provide reliable homing/guidance updates.[1–7]

Presented as Paper 96-2322 at the AIAA 27th Plasmadynamics and Lasers Conference, New Orleans, LA, June 17–21, 1996; received July 10, 1996; revision received July 14, 1997; accepted for publication July 15, 1997.

*Principal Aeronautical Engineer, Hypersonic Aerodynamics and Propulsion Branch. Member AIAA.

It is evident that guidance errors can result from aerodynamic and aerothermal effects, and homing concept development must address all of these issues. Therefore, codes must be developed and validated to ensure an understanding of and a predictive capability for the analysis of all phenomena capable of affecting microwave sensor performance. Such validation tasks necessarily require a database. Such a database can be obtained from dedicated experiments performed in a test facility that is capable of generating some of the aerodynamic and aerothermal conditions wherein plasma–environment isues, including angle-of-attack (AOA) effects, can be quantitatively examined in a well-conceived laboratory measurements program.

This paper summarizes the experiment design, performance techniques, and the results of a test program whose objective was to develop a database on the interaction of L-band (rf) electromagnetic radiation with the ionized flowfield about a re-entry vehicle, for purposes of analytic code validation. However, presented here are the results obtained from the electrostatic probe surveys and the aerothermal measurements. The experiments were performed in the Calspan 96-in. Hypersonic Shock Tunnel wherein plasma conditions were generated aerodynamically, in the test vehicle flowfield under laminar flow conditions appropriate to high-altitude re-entry.

Design of the Experimental Program

Experimental Facilities

This experimental program was conducted in Calspan's 96-in. shock tunnel at nominal freestream Mach number of 9.3 and at a Reynolds number of 1.5×10^5/m (0.5×10^6/ft). A photograph of the facility is shown in Fig. 1. This facility is a large conventional reflected shock tunnel in which the flow is initiated by rupturing a double diaphragm, permitting high-pressure hydrogen from the driver section to expand rapidly into the driven section containing the test gas (air). This sudden release of pressure generates a normal shock, which propagates through the low-pressure air, producing a region of high-temperature, high-pressure air between this normal-shock front and the gas interface (the contact surface) between the driver and driven gases. When the primary, or incident, shock strikes the end of the driven section, it is reflected, leaving a reservoir region of almost stationary, high-pressure, heated air. This air is then expanded through a nozzle to the desired freestream conditions in the test section. The duration of the flow in the test section is controlled by the interactions between the reflected shock, the interface, and the leading expansion wave generated by the nonstationary expansion process occurring in the driver section. It is standard operating procedure to control the initial conditions of the gases in the driver and driven sections so that the gas interface becomes transparent to the reflected-shock interaction. This is known as operating under tailored-interface conditions. Under these conditions, the test time is controlled by the time taken for the driver/driven interface to reach the throat, or the leading expansion wave to decrease the reservoir

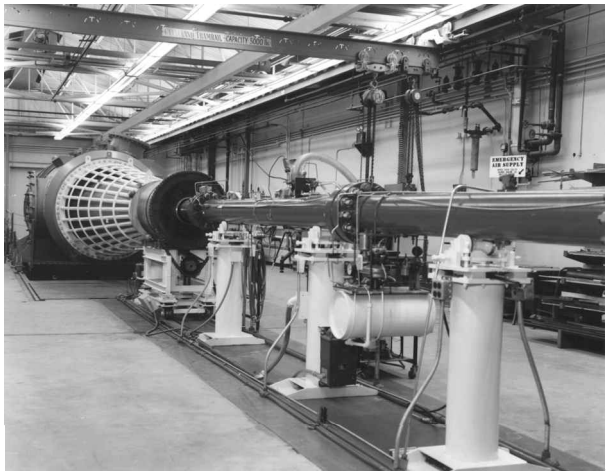

Fig. 1 Calspan 96-in. Hypersonic Shock Tunnel.

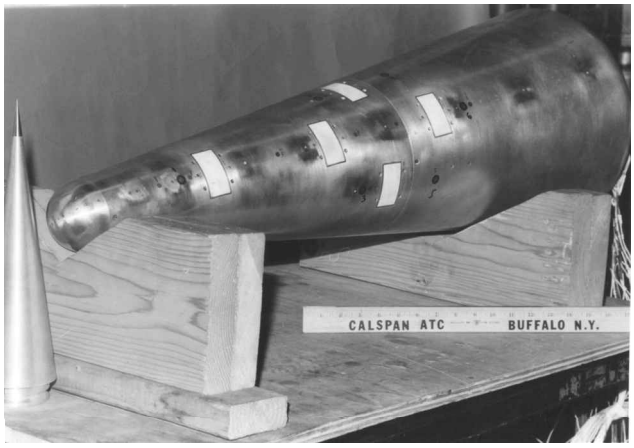

Fig. 2 Full-scale re-entry vehicle test model with changeable nose tip.

of pressure behind the reflected shock. Thus, the flow duration is either driver-gas limited or expansion-wave limited, respectively.

Test Model Description

The model used in this experimental study was a 7.8-deg half-angle cone with interchangeable nose tips. On the basis of blunt body flowfield analyses, the model geometry selected for the tests used the spherically blunted cone with a nose radius of 4.32 cm (1.7 in.). The total test model length is about 1 m (3 ft). The model was supported in the shock tunnel test section by a specially designed crank-angle sting installed into the test section mount. All test model orientations were effected via pin location selection, which permitted a choice of crank angles of 0, 2, 6, and 13 deg. The sting could be rotated to allow combinations of pure pitch, yaw, and combinations of both. A photograph of the test model is shown in Fig. 2.

Aerothermal Instrumentation

The test model was instrumented with a total of 26 heat transfer gauges and 20 high-frequency pressure transducers. The instrumentation locations are shown in schematic in Fig. 3. The hemispherical nose had five pressure locations including the stagnation point. The nose was also fitted with five coaxial thermocouple type heat transfer gauges. The remainder of the heat transfer gauges distributed along the conical surface of the model were Calspan fabricated platinum thin-film resistance thermometers. The model surface also included six circular-section flush-mounted current collecting probes.

Thin-Wire Electrostatic Probe Instrumentation

Thin-wire electrostatic voltage-swept probes were used to measure the electron temperature and number density in the shock layer and the boundary-layer regions of the test model flowfield. Each probe consists of a short length of tungsten wire approximately 0.076 mm (0.003 in.) in diameter with a length to diameter ratio of 80. The probes were oriented so that they were always aligned

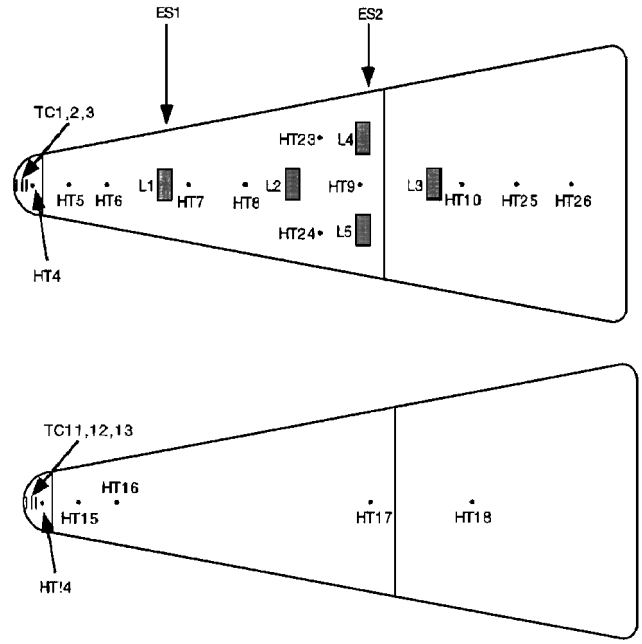

Fig. 3 Schematic of the test model instrumentation and antenna locations.

with the flow direction during a test run. In operation, the voltage applied to the probes was swept from −5 to +3 V to record both the ion collecting and retarding field regions of the probe characteristic. Under suitable conditions of collision frequency, the current-probe behavior in these regions provide both the ion number density and the electron temperature. The choice of wire size affects the important ratios of probe size to electron neutral and ion neutral mean free paths, which will in turn determine whether free-molecular, transitional, or collisional sheath considerations would have to be invoked for proper data reduction. The selection of test conditions for this experimental research program allowed the application of collisionless free-molecular probe theory data reduction techniques.

The point determination of the electron number density n_e and temperature T_e in a moving plasma is an intrusive measurement, performed by means of a swept-voltage, thin-wire probe. Several such probes may be installed in a common rake; each probe aligned with the local flow direction and positioned at different distances off the vehicle surface so as to measure the number density profile through the boundary layer.

A linear voltage ramp is simultaneously applied to each probe, swept over a voltage range, e.g., from −5 to +3 V sufficient to record both the ion current and the electron retarding field regions of the probe characteristic. An illustrative sketch of a complete electrostatic probe characteristic is shown in Fig. 4.

In the interpretation of the probe characteristic, the ion current collected by the probe at a selected (nondimensional) probe potential is used, in conjunction with the measured electron temperature, to derive the local ion number density corresponding to the collected ion current. Probe data reduction follows the theory of Laframboise[8] for the case of a collisionless (free-molecular) sheath.

A nondimensional probe potential χ_p is defined by

$$\chi_p = (e/kT_e)(V_p - V_\infty) \tag{1}$$

which is the dimensionless difference between the probe potential V_p and the plasma potential V_∞. The latter is the potential at which the probe collects both ions and electrons (random currents) without the aid of electric fields. In the equation for χ_p, e is the electron charge, k is the Boltzmann constant, and T_e the electron temperature.

Laframboise's results from the collected ion and electron current densities at negative values of χ_p are written as

$$j_i = en_e(kT_e/2\pi m_i)^{\frac{1}{2}} i_+ \tag{2}$$

$$j_e = en_e(kT_e/2\pi m_e)^{\frac{1}{2}} \chi_p \tag{3}$$

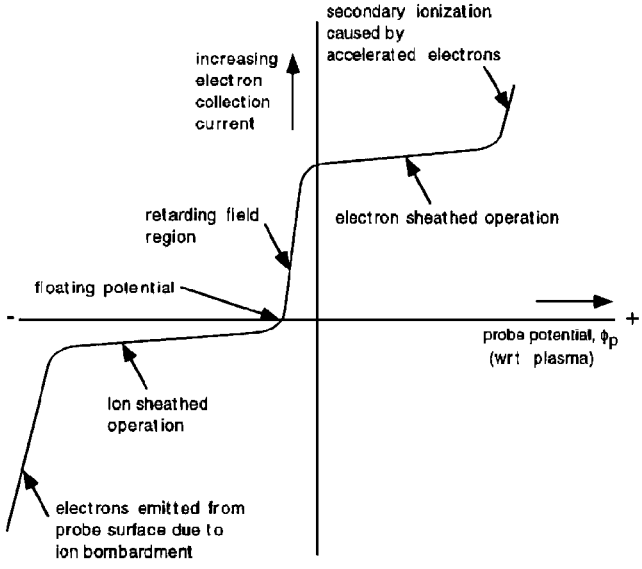

Fig. 4 Sketch of the electrostatic probe characteristic.

where i_+ is a normalization factor representing the increase in the collected ion current over the random kinetic ion flux to the probe at $\chi_p \to 0$, i.e., at the plasma potential. The factor i_+ is a function of χ_p, the ratio of the probe radius to Debye length r_p/λ_D, and the ratio of ion to electron temperatures. The Debye length (in centimeters) is given by

$$\lambda_D = \left(\frac{\varepsilon_0 k T_e}{n_e e^2}\right)^{\frac{1}{2}} \approx 6.9\sqrt{\frac{T_e}{n_e}} \tag{4}$$

When the voltage applied to the probe is swept from negative toward positive values, $\chi_p \to 0$ and the electron current collected by the probes increases rapidly because the higher thermal velocities of the electrons enable them to reach the probe surface in spite of the repelling voltage. This region of the probe characteristic is called the retarding-field region. Differentiating Eq. (3),

$$\frac{\mathrm{d}\ell n(j_e)}{\mathrm{d}V_p} = \frac{e}{kT_e} \tag{5}$$

i.e., the slope of a semilog plot of retarding-field region probe current vs probe voltage is e/kT_e, which is the basis for the determination of the electron temperature. Then

$$T_e = \frac{11{,}600}{e/kT_e} \tag{6}$$

The ion number density is obtained from the ion-current portion of the probe characteristic at large negative values of χ_p ($\chi_p < -10$), via Eq. (2). The calculation of number density from the measured ion current density is seen to involve the ion mass m_i, hence, the identity, of the collected ion. In a pure-air plasma, this may be assumed to be NO^+. In re-entry vehicle boundary-layer flows, alkali-metal contaminant ionization from ablating surfaces can become a predominant free-electron source. In the case of flight diagnostic measurements, therefore, the probe voltage ramp excursion should be extended sufficiently to record the electron-sheathed region of the probe characteristic.

At positive probe potentials, the electron number density n_e is measured independently of the nature of the collected ion. Because $n_e \equiv n_i$ for a neutral plasma, this can further afford a means of corroborating the identity of the ion in the flow. Such use of thin-wire electrostatic probes has been studied in shock tunnel flows.[9] Therein, the charged-particle densities determined from the ion-sheathed and electron-sheathed portions of the probe characteristic were in good agreement with each other and with independent microwave interferometer measurements.

In relating χ_p to the corresponding probe potential V_p, it can be difficult to define the plasma potential V_p from the probe characteristic with precision. Instead, the nondimensional probe potentials can be referred to the floating potential V_F, which is readily identifiable on each probe characteristic as the probe voltage for zero net collected current.

Thus, by equating Eqs. (2) and (3) at $\chi = \chi_F$,

$$e^{\chi_F} = (m_e/m_i)^{\frac{1}{2}} i_+ \tag{7}$$

or

$$\chi_F = (e/kT_e)(V_F - V_\infty) = \tfrac{1}{2}\ell n(m_e/m_i) i_+ \tag{8}$$

Because the effect on χ_F is small, i_+ is taken as unity. Then,

$$\chi_p = (e/kT_e)(V_p - V_\infty) + \chi_F \tag{9}$$

and

$$V_p = \frac{\chi_p - \ell n(m_e/m_i)^{\frac{1}{2}}}{e/kT_e} - V_F = \frac{\chi_p + 5.4}{e/kT_e} + V_F \tag{10}$$

for the NO^+ ion.

The ion number density cannot be obtained directly from Eq. (2) because i_+ depends on r_p/λ_D, which is also dependent on number density. The determination of the number density using the theory of Laframboise[8] has followed the method of Sonin,[10] which eliminates the need for an iterative calculation. From Eq. (2),

$$n_e i_+ = (1/e)(2\pi m_i/e)^{\frac{1}{2}} j_i \tag{11}$$

which, following substitution for n_e in terms of the Debye length [Eq. (4)] can be written

$$(r_p/\lambda_D)^2 = \left(r_p^2/\varepsilon_0\right)(2\pi m_i/e)^{\frac{1}{2}}(e/kT_e)^{\frac{3}{2}} j_i \tag{12}$$

where ε_0 is the vacuum permittivity (8.854×10^{-12} F m^{-1}). As noted by Sonin, this expression is not explicitly dependent on the number density. In terms of the quantities measured using the electrostatic probes, where $j_i = I_i/2\pi r_p \lambda_D$, Eq. (12) can be rewritten as

$$\begin{aligned}(r_p/\lambda_D)^2 i_+ &= (1/\varepsilon_0)(m_i/2\pi e)^{\frac{1}{2}}(r_p/\lambda_p)(e/kT_e)^{\frac{3}{2}} I_i \\ &= 25.1(r_p/\lambda_p)(e/kT_e)^{\frac{3}{2}} I_i\end{aligned} \tag{13}$$

for the NO^+ ion, where I_i is the ion current (in microamperes) at large negative χ_p.

From computed values of $(r_p/\lambda_D)^2 i_+$, the corresponding values of i_+ for given χ_p are obtained from a plot of Laframboise's[8] results for the case $T_i/T_e = 1.0$. The value of i_+ is, in fact, not very sensitive to the value for T_i/T_e. Therefore, once e/kT_e is determined from the probe characteristic [Eq. (5)], the probe potential corresponding to the selected negative χ_p is evaluated from Eq. (10). The value of $(r_p/\lambda_D)^2 i_+$ is calculated using Eq. (13) and the corresponding value of i_+ is obtained from plots of $(r_p/\lambda_D)^2 i_+$ vs i_+ at selected χ_p. The ion number density per cubic centimeter is then determined as

$$n_i = \left(1/e^{\frac{3}{2}}\right)(m_i/2\pi)^{\frac{1}{2}}(e/kT_e)^{\frac{1}{2}}(1/r_p\lambda_D)(I_i/i_+) \tag{14}$$

or

$$n_i = 1.4(10^7)(e/kT_e)^{\frac{1}{2}}(I_i/i_+)(1/r_p\lambda_D) \tag{15}$$

for NO^+ and I_i in microampere, $r_p\lambda_D$ in centimeters squared.

The slope measurement for the determination of e/kT_e should be made at a point where the ion current is negligible. It has been shown that the net current to the probe is essentially equal to the electron current when the latter is about twice the ion current collected at large negative χ_p. In the reduction of the electrostatic probe data from these experiments, the ion currents employed were for probe potentials corresponding to nondimensional χ_p values of -15 and -20. The slopes of the semilog I_p vs V_p plots were then evaluated

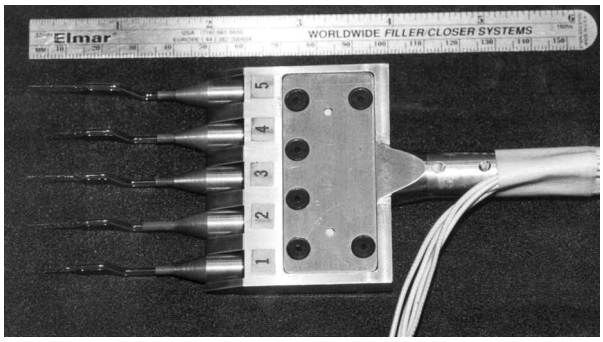

Fig. 5 Photograph of the thin-wire electrostatic probe rake.

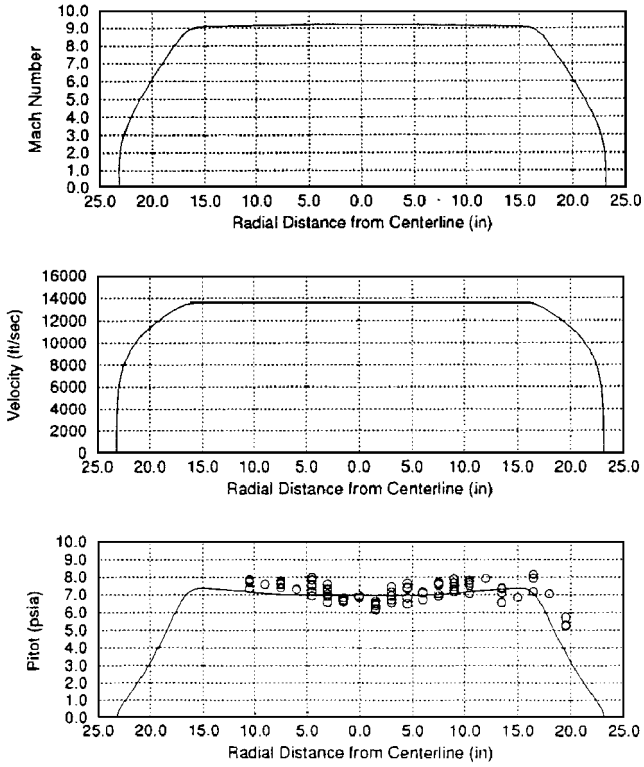

Fig. 6 Test conditions for the experimental tests with pitot pressure measurements.

at probe current at least twice the magnitude of the ion currents measured at the negative χ_p values.

A five-probe rake was employed for these studies. The rake was always positioned in the flowfield over the cone surface opposite that containing the active rf antennas so as not to interfere with the rf measurements. A photograph of the rake is shown in Fig. 5. The rake was moved during the course of the study to provide profile measurements at different axial locations along the model for various vehicle orientations. In addition, a two-probe rake was located in the wake region behind the model.

Results and Discussion

Test Stream Diagnostics and Condition

In addition to the test matrix just described, a series of airflow tests were conducted to describe the freestream quantities and quality. A highly instrumented airflow survey rake included: stagnation heat transfer probes and pitot pressure probes. In addition to the airflow series, a Navier–Stokes computation of the nozzle expansion was calculated from the reservoir (driven tube) to the freestream core flow. These results are plotted with pitot values from several of the airflow tests in Fig. 6. Repeatability of the test point is considered to be quite good, as can be seen from these measurements of the pitot. In addition to the pitot values, a plot of the exit plane Mach number and velocity are included. The test point to which these data

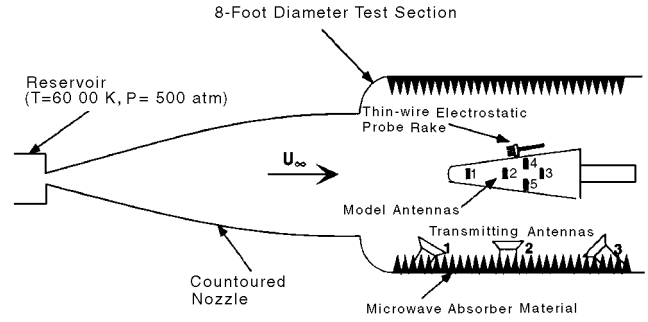

Fig. 7 Schematic of the experimental configuration in the shock tunnel.

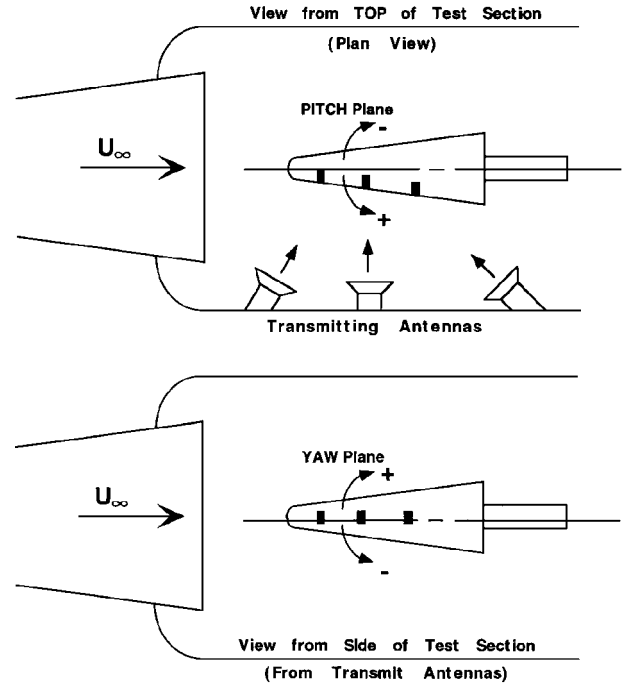

Fig. 8 Test model orientation and sign convention.

correspond is a simulation of 140 kft (42.7 km) density altitude at 14,350 ft/s (4.4 km/s).

Aerothermal Surface Measurements

A total of 33 test runs were made in the basic test program with the test model. The matrix is shown in Table 1. The matrix includes variation of AOA with several combinations of pitch and yaw. Also included was a single test with a sharp nose to give a baseline for the absence of significant plasma number density in the flowfield. Figure 7 shows the experimental setup in the Calspan 96-in. Hypersonic Shock Tunnel, and Fig. 8 illustrates the test model orientation and sign convention used for the experiments.

Figure 9 shows the pressure data for the 0-deg AOA case. The data indicate the results for three separate test runs and show good repeatability of the test flowfield. Figures 10 and 11 show the data for the 2- and 6-deg pure pitch cases. The results indicate clearly the differences between the leeward and windward sides of the model and also repeat very well. In general, repeatability of the pressure data was very good. The surface heat transfer data are presented in a manner similar to the surface pressure data (Figs. 12–14). Wherever possible, repeat test runs are incorporated into the same plot to show the consistency in the data set.

Electron Number Density Measurements

Electron number density profiles were obtained with thin-wire electrostatic probes. Two profile locations were selected that correspond to the forwardmost antenna location (ES-1) and the midpoint between the second and third in-line antenna positions (ES-2). Figure 3 shows the location of the probes in relation to the rf antennas

Table 1 Experimental test matrix

Test run number	Attack	Model position, deg Pitch	Yaw
1	0	0	0
2	0	0	0
3	0	Sharp	Nose
4	2	2	0
5	2	2	0
6	2	2	0
7	6	6	0
8	6	6	0
9	2	−2	0
10	2	−2	0
11	6	−6	0
12	6	−6	0
13	2	0	2
14	2	0	2
15	6	0	6
16	6	0	6
17	6	−4.2	4.2
18	6	−4.2	4.2
19	2	−1.4	1.4
20	2	−1.4	1.4
21	2	1.4	−1.4
22	2	1.4	−1.4
23	6	4.2	−4.2
24	6	4.2	−4.2
25	0	0	0
26	6	−6	0
27	6	−6	0
28	6	−6	0
29	2	−2	0
30	2	−2	0
31	13	−13	0
32	13	13	0
33	0	0	0

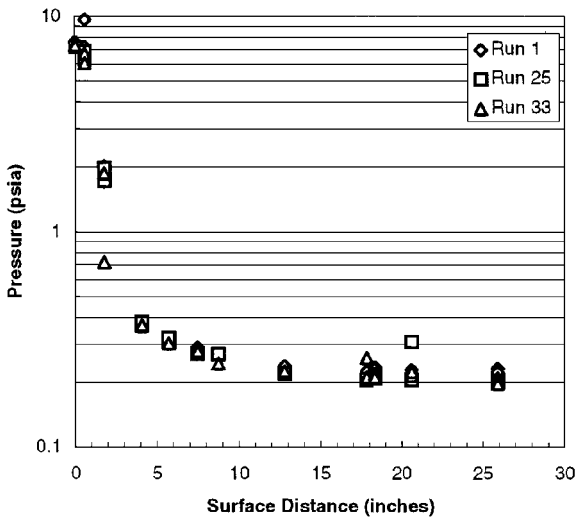

Fig. 9 Measured test model pressure at 0-deg AOA.

and from the nose of the test model. Essentially, the data were obtained by ramping a voltage linearly from −5 to +3 V over a 100-μs time period. Four of these ramps were sequenced during a single test run to ensure synchronization with the steady test flow interval. During the performance of the tests, the timing of the airflow over the model provided in many cases two of the input ramps during the test period. Selected profiles are presented here to show the trends and typical profile behavior.

Figure 15 shows the electron number density profiles for test runs 25 and 33. These test runs represent repeat data for the 0-deg AOA case at the forward position identified by ES-1. This position is 19.8 cm (7.8 in.) along the surface from the nose of the hemisphere/cone model. These two tests give a good indication of the repeatability of the test flow. The profile shapes from the two runs are nearly the

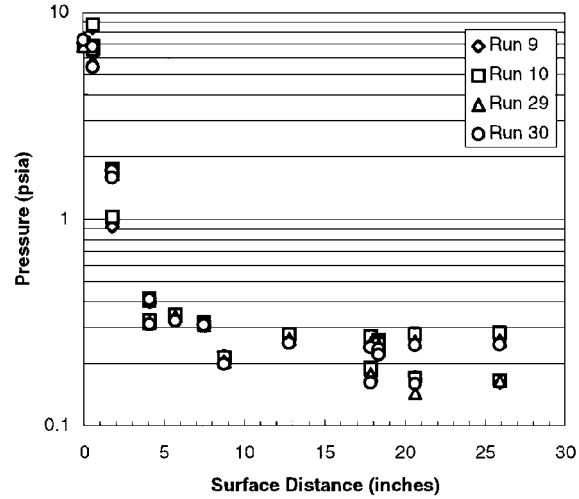

Fig. 10 Measured test model pressure at 2-deg AOA.

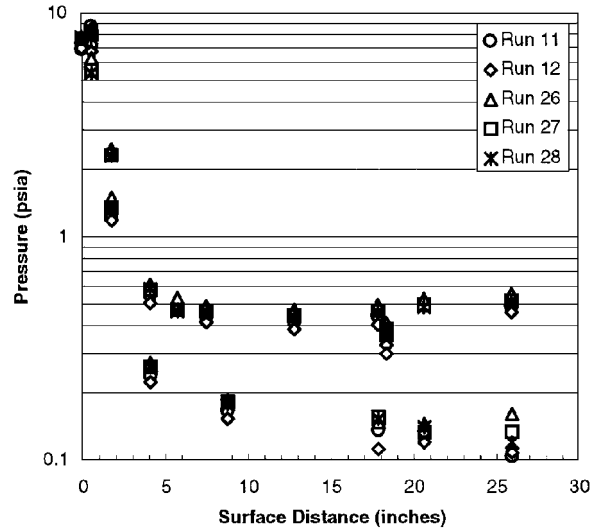

Fig. 11 Measured test model pressure at 6-deg AOA.

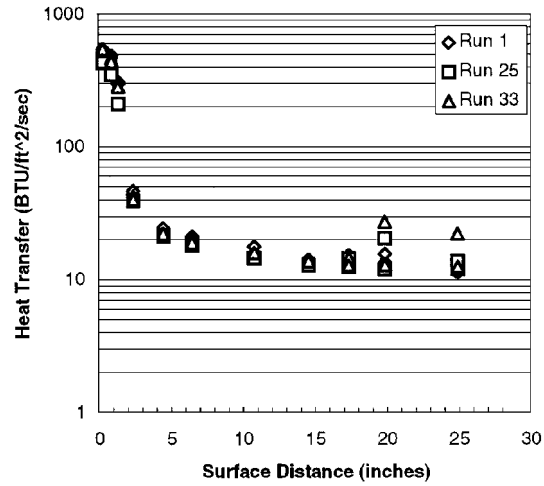

Fig. 12 Measured test model heat transfer at 0-deg AOA.

same with the peak number density level located approximately 0.25 cm (0.1 in.) above the model surface at a density level of slightly greater than $1.0e10^{11}$ cm^{-3}. Figure 15 also shows the number density data for 0-deg AOA for the ES-2 position, which is located 47 cm (18.5 in.) from the nose of the model. In this case, the data are somewhat sparse; however, the number density levels are nearly the same as in the ES-1 position data with an indication of a thicker plasma layer, possibly up to 0.4 cm (0.16 in.) above the model surface.

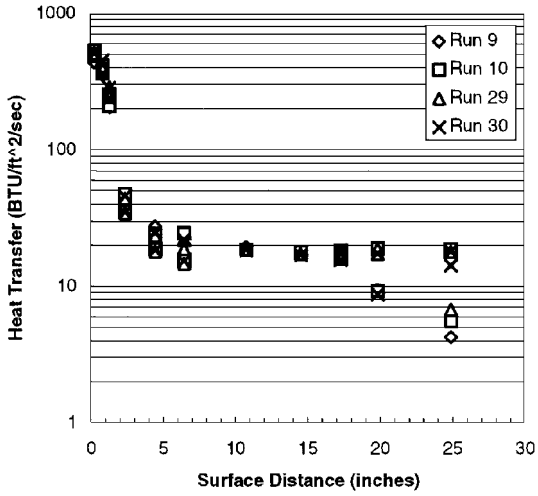

Fig. 13 Measured test model heat transfer at 2-deg AOA.

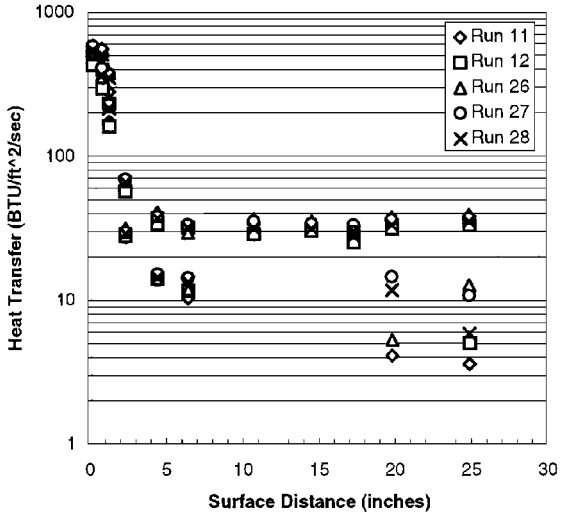

Fig. 14 Measured test model heat transfer at 6-deg AOA.

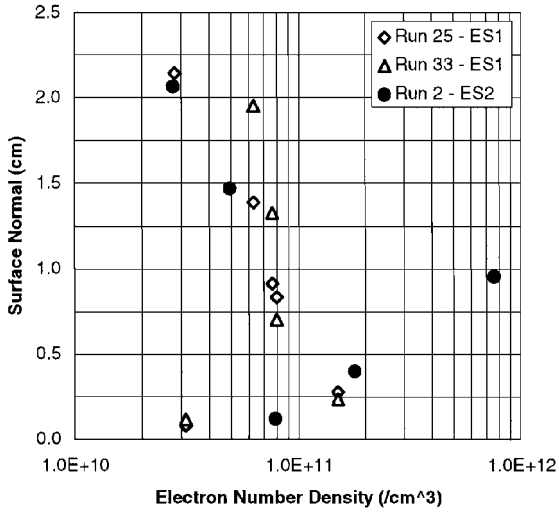

Fig. 15 Measured electron number density at 0-deg AOA.

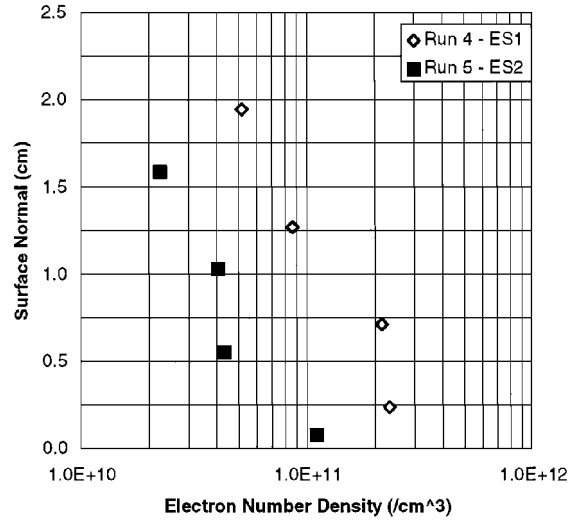

Fig. 16 Measured electron number density at +2-deg AOA, windward.

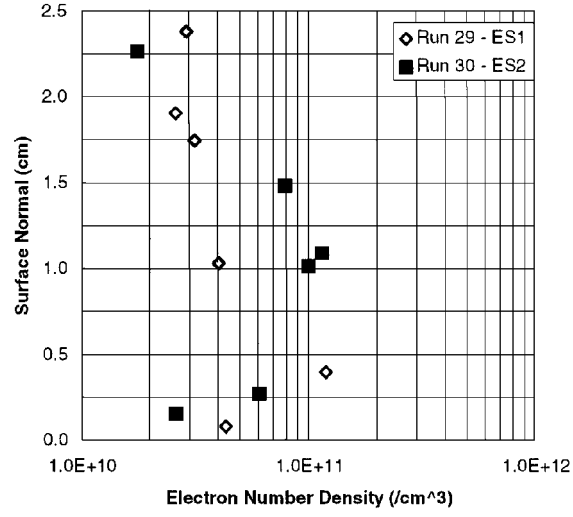

Fig. 17 Measured electron number density at +6-deg AOA, windward.

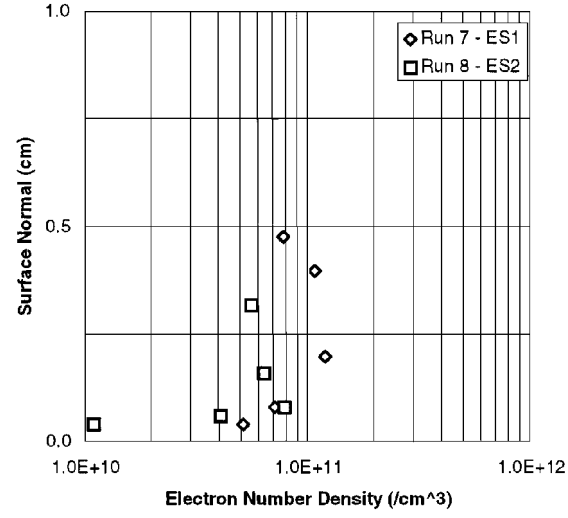

Fig. 18 Measured electron number density at − 2-deg AOA, leeward.

The following discussion regarding electron number densities at various AOAs follows the convention shown in Fig. 8. Positive pitch indicates electron number densities measured on the windward side of the vehicle, and negative pitch relates to leeward measurements. In general, the windward layer is thin relative to the leeward layer, and also it is thin in some cases relative to the resolution obtainable with the probe rake used to collect the data. Therefore, in some cases the resolution of the windward data is not sufficient to completely describe the profile shape. Figure 16 shows the windward data collected for the +2-deg pitch orientation. At the ES-1 position, the peak level is approximately $2.5e10^{11}\,cm^{-3}$ and the peak level is decreased back to the ES-2 position to $1.1e10^{11}\ cm^{-3}$. The distance above the surface for the peak level is not very discernible at this position. The +6-deg pitch or windward data include two test runs and are shown in Fig. 17. At the ES-1 position at peak level slightly less than 10^{11} is indicated. A slightly higher level is shown for the ES-2

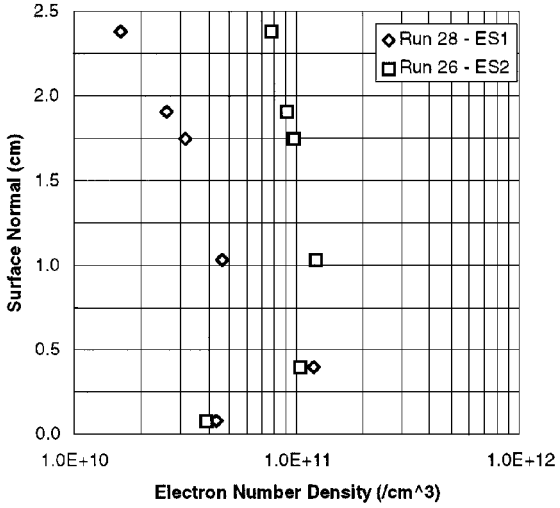

Fig. 19 Measured electron number density at − 6-deg AOA, leeward.

position; however, the resolution for these profiles is most likely insufficient to describe the layer completely because the thickness of the layer appears to be less than 0.5 cm (0.2 in.).

On the leeward side of the model, the plasma sheath is thicker and better defined by the thin-wire probe measurements. Figure 18 shows the data collected for the −2-deg pitch case. At the ES-1 position, a peak electron number density of $1.1e10^{11}$ at 0.14 in. (0.35 cm) above the surface is observed. Farther back, at the ES-2 position, the peak in the profile is seen to have moved out near 0.4 in. (1.0 cm) from the surface. The −6-deg pitch data (Fig. 19) show similar peak numbers at slightly greater than $1.0e10^{11}$ cm^{-3} at the ES-1 position at 0.4 cm above the surface of the model. At the ES-2 position, an indication of a thickening of the layer with the peak number density observed approximately 1.0 cm off the surface at the same level ($1.0e10^{11}$ cm^{-3}) as the ES-1 position.

Conclusions

A comprehensive shock tunnel program has been performed on the quantitative measurement of the plasma environment about a full-scale hypervelocity re-entry vehicle. The shock tunnel operating conditions generated freestream test flow velocity at approximately 4.3 km/s (14,000 ft/s), with an equivalent density altitude of 42.7 km (140,000 ft). The measurements, performed in laminar flow conditions, comprise a database of the flowfield plasma profiles and test model surface aerothermal properties.

The overall experimental objectives were achieved in providing a comprehensive database on the effects of AOA of a hypersonic vehicle on the measured electron number density profiles in the shock layer, the measured surface pressure, and heat transfer rate distributions. The data exhibited both good repeatability and were fully consistent with the responses expected for the change in flowfield environment produced by the changes in vehicle attitude.

Acknowledgments

This work was supported by the U.S. Air Force Phillips Laboratory (AFMC), Hanscom Air Force Base, Massachusetts, under Contract F19628-94-C-0015. The author would like to acknowledge the valuable efforts made by many to the success of this program. Many thanks go to Emmett Sutton of Concord Sciences Corp., whose experience with electron density measurements was very helpful. Many thanks go also to Robert Morris of Phillips Laboratory, who served as program monitor and advisor.

References

[1]Boyer, D. W., "Re-Entry Vehicle Flowfield Plasma Effects, Including Angles of Attack on RF Uplink Signal Propagation and Mutual Coupling," Calspan, Rept. 7515-4, BMO-TR-91-21, Buffalo, NY, May 1991.

[2]Boyer, D. W., "Measured Surface Heat Transfer Rate Distributions for Model Attitude Orientations During RF Interaction Experiments," Calspan, Rept. 7515-3, Buffalo, NY, Oct. 1990.

[3]Boyer, D. W., "Measured Electron Number Density Profiles in the Model Flowfield During RF Interaction Experiments," Calspan, Rept. 7515-2, Buffalo, NY, July 1989.

[4]Boyer, D. W., "Design of a Laboratory Measurements Program for the Investigation of Flowfield Plasma Effects on a Microwave Homing Vehicle," Calspan, Rept. 7437-1, Buffalo, NY, Jan. 1988.

[5]Dunn, M. G., and Lordi, J. A., "Measurement of Electron Temperature and Number Density in Shock Tunnel Flows. Part II NO^+ and e^- Dissociative Recombination Rate in Air," *AIAA Journal*, Vol. 7, No. 11, 1969, p. 2099.

[6]Chadwick, K. M., Boyer, D. W., and Andre, S. N., "Plasma and Flowfield Induced Effects on Re-Entry Vehicles for L-Band at Near Broadside Aspect Angles," U.S. Air Force Phillips Lab., Rept. PL-TR-2094, Hanscom AFB, MA, Sept. 1996.

[7]Chadwick, K. M., Boyer, D. W., and Andre, S. N., "Plasma and Flowfield Induced Effects on Hypervelocity Re-Entry Vehicles for L-Band Irradiation at Near Broadside Aspect Angles," AIAA Paper 96-2322, June 1996.

[8]Laframboise, J. G., "Theory of Spherical and Cylindrical Langmuir Probes in a Collisionless, Maxwellian Plasma at Rest," Univ. of Toronto Inst. for Aerospace Studies, Rept. 100, Toronto, ON, Canada, March 1966.

[9]Dunn, M. G., "Use of Positively Biased Electrostatic Probes to Obtain Electron Density in Collisionless Flows," *AIAA Journal*, Vol. 10, No. 8, 1972, p. 996.

[10]Sonin, A. A., "The Behavior of Free Molecular Cylindrical Langmuir Probes in Supersonic Flows, and Their Application to the Study of the Blunt Body Stagnation Layer," Univ. of Toronto Inst. for Aerospace Studies, Rept. 109, Toronto, ON, Canada, Aug. 1965.

I. D. Boyd
Associate Editor